ACS OMEGA

http://pubs.acs.org/journal/acsodf

Article

Role of Dispersion Interactions in Endohedral TM@$(ZnS)_{12}$ Structures

Elisa Jimenez-Izal,* Iker Ortiz de Luzuriaga, Eloy Ramos-Cordoba, and Jon M. Matxain

Cite This: *ACS Omega* 2021, 6, 16612−16622

Read Online

ACCESS | Metrics & More | Article Recommendations | Supporting Information

ABSTRACT: II−VI semiconducting materials are gaining attention due to their optoelectronic properties. Moreover, the addition of transition metals, TMs, might give them magnetic properties. The location and distance of the TM are crucial in determining such magnetic properties. In this work, we focus on small hollow $(ZnS)_{12}$ nanoclusters doped with TMs. Because $(ZnS)_{12}$ is a cage-like spheroid, the cavity inside the structure allows for the design of endohedral compounds resembling those of C_{60}. Previous studies theoretically predicted that the first-row TM$(ZnS)_{12}$ endohedral compounds were thermodynamically unstable compared to the surface compounds, where the TM atom is located at the surface of the cluster. The transition states connecting both structure families were calculated, and the estimated lifetimes of these compounds were predicted to be markedly small. However, in such works dispersion effects were not taken into account. Here, in order to check for the influence of dispersion on the possible stabilization of the desired TM$(ZnS)_{12}$ endohedrally doped clusters, several functionals are tested and compare to MP2. It is found that the dispersion effects play a very important role in determining the location of the metals, especially in those TMs with the 4s3d shell half-filled or completely filled. In addition, a complete family of TM doped $(ZnS)_{12}$ nanoclusters is explored using *ab initio* molecular dynamics simulations and local minima optimizations that could guide the experimental synthesis of such compounds. From the magnetic point of view, the Cr(^{7}S)@$(ZnS)_{12}$ compound is the most interesting case, since the endohedral isomer is predicted to be the global minimum. Moreover, molecular dynamics simulations show that when the Cr atom is located at the surface of the cluster, it spontaneously migrates toward the center of the cavity at room temperature.

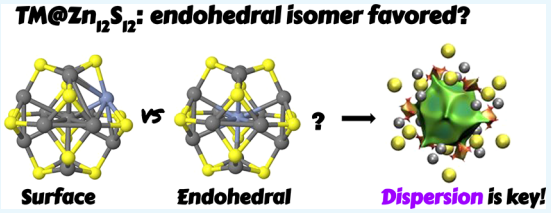

1. INTRODUCTION

II−VI semiconductors have been extensively studied in the last decades due to the optoelectronic properties that make them suitable for important applications in photocatalysis,[1] solar cells,[2,3] or quantum devices.[4,5] Likewise, the use of II−VI semiconductor nanomaterials in biological investigations has increased notably due to their unique optical properties and to recent advances in biofunctionalization.[6] The addition of transition metals, TMs, can change the structural and electronic properties of these materials[7−10] and even give them magnetic properties.[11,12] The resulting magnetic and optoelectronic properties are assorted and dependent on the particular transition metal atom.[13−19]

II−VI nanomaterials often exhibit new and exciting properties, arising from the quantum confinement and their high surface to volume ratio. Moreover, nanoclusters composed of a few atoms are treatable by first-principles computational protocols allowing the study of their properties at the atomic level, that would otherwise be extremely difficult to explore in larger nanoparticles. For instance, the endohedral doping of $(ZnS)_{12}$, that has spherical symmetry, can be considered as equivalent to the interstitial doping in bulk. A recent review highlights the importance of such endohedrally doped nanoclusters.[20]

Several TM doped $(ZnS)_{12}$, $(CdS)_{12}$, and $(ZnO)_{12}$ clusters have been studied theoretically in the past.[9,21−27] Previously some of us theoretically characterized the first- and second-row TM endohedrally doped $(ZnS)_{12}$ and $(ZnS)_{16}$ nanoclusters.[11,28,29] From all the compounds, the most promising ones were predicted to be those endohedrally doped with silver. Although metastable, Ag@$(ZnS)_i$ were predicted to have sufficiently large lifetimes and show interesting magnetic properties and coupling when forming Ag@$(ZnS)_i$ dimers, directly related to the Ag−Ag distance. Indeed, for the Ag@$(ZnS)_{12}$ dimer, Ag atoms exhibit an antiferromagnetic coupling, while for the larger Ag@$(ZnS)_{16}$ dimer, ferromagnetic and antiferromagnetic states are degenerate.[11] Unfortunately, in the rest of the TM doped clusters (except for Zn and Cu that do not have magnetic properties), it was found that the metal atom moves toward the surface of the nanocluster, breaking it and forming the more stable surface doped structure (see Figure 1).

Electronic structure theory is fundamental for the prediction and understanding of molecules and materials. Importantly, the reliability of the approximate electronic structure method lies in its capability to describe all the interaction energy components, such as the electrostatic and dispersion

Received: April 15, 2021
Accepted: May 25, 2021
Published: June 17, 2021

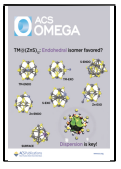

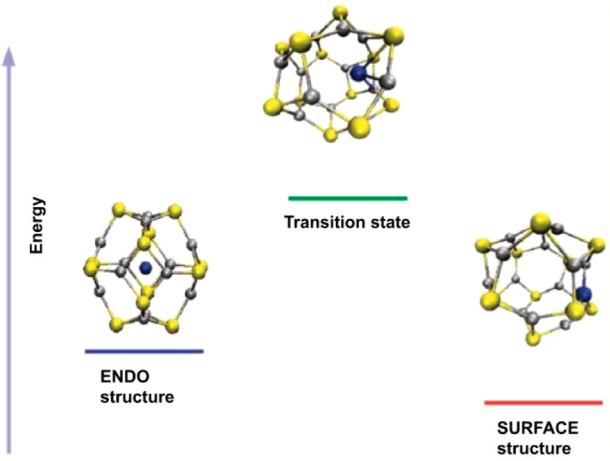

Figure 1. General picture for TM@$(ZnS)_{12}$ structures, where surface compounds are more stable than their endohedral counterparts.

interactions. The methodology used in the previous studies on TM doped $(ZnS)_{12,16}$ nanoclusters (B3LYP), however, did not account for van der Waals interactions. Notice that the TM−cage interaction in the endohedral isomers tends to be weak, and consequently, the lack of specific consideration of dispersion may lead to the underestimation of the stability of the endohedral compounds.

The main goal of this work is to establish the importance of dispersion interactions for the correct description of such systems and to test whether the dispersion could stabilize the endohedral isomers. With this aim, first different DFT functionals are compared to a reference MP2 calculation. Then the selected DFT functional is used to revisit the stability of endohedral compounds of selected first-row $TM(ZnS)_{12}$ by means of quantum dynamics along with an exhaustive search of the potential energy surface. Characterizing new potentially stable endohedral TM@$(ZnS)_{12}$ compounds might lead to the discovery of novel magnetic nanostructures, with very promising implications in technological applications such as spintronics.

2. METHODS

All the geometry optimizations and frequency calculations were done using the Gaussian16 package.[30] Harmonic vibrational frequencies were obtained by analytical differentiation of gradients, to identify whether the characterized structures were true minima or transition states. Such frequencies were then used to evaluate vibrational corrections to Gibbs free energy, using the standard procedure of Gaussian16 (see the Supporting Information). For sulfur and zinc atoms, the relativistic compact effective core potentials and shared-exponent basis set of Stevens, Krauss, Basch, and Jasien (SKBJ)[31] were used, and the fully relativistic pseudopotentials, with 10 electrons in the core, developed by Dolg et al.,[32,33] were used for the rest of the TM. The reference method to account for the dispersion is the second-order Møller−Plesset theory (MP2).[34−38] We must highlight that the MP2 method is not the most accurate wave function based method, but for the systems studied here it is affordable, unlike other post Hartree−Fock methods such as Coupled Cluster. Several DFT functionals were compared to MP2: B3LYP,[39] CAM-B3LYP,[40] M06,[41] M06-2X,[41] wB97X-D,[42] PBE[43,44] combined with the D3 version of Grimme's dispersion with Becke−Johnson damping,[45] denoted hereafter as PBE-D3BJ, and a set of double-hybrid methods, including exact HF exchange with an MP2-like correlation to DFT calculations. Concretely, the following double-hybrid functionals have been used: B2PLYP[46] and mPW2PLYP[47] methods, developed by Grimme, and their corresponding empirical dispersion corrected[48] counterparts B2PLYPD and mPW2PLYPD. In addition, B2PLYPD3 which combines the B2PLYP method with Grimme's D3BJ dispersion,[45,49] DSDPBEP86,[50,51] a dispersion-corrected double-hybrid functional with Grimme's D3BJ dispersion, and the PBE0DH[52] and PBEQIDH[53] double-hybrid functionals.

B3LYP was chosen because it is the functional used in previous works, and as CAM-B3LYP, it does not include dispersion corrections.[11,28,29] Both M06 and M06-2X are supposed to describe van der Waals interactions by construction, and wB97X-D includes an empirical atom−atom dispersion potential. Double-hybrid functionals will help

Table 1. Free Energy Differences between *ENDO* and *SURFACE* Structures ($\Delta G_{S\text{-}E}$) and *ENDO* and Transition State Structures (ΔG_{TS}), in kcal/mol, for ^{5}Ti, ^{7}Cr, ^{3}Ni, and ^{1}Zn Doped $(ZnS)_1$ Nanoclusters[a]

	^{5}Ti		^{7}Cr		^{3}Ni		^{1}Zn	
	$\Delta E_{S\text{-}E}$	ΔE_{TS}	$\Delta E_{S\text{-}E}$	ΔE_{TS}	$\Delta E_{S\text{-}E}$	ΔE_{TS}	$\Delta E_{S\text{-}E}$	ΔE_{TS}
MP2	5.58	5.38	19.80	16.57	8.74	−2.10	27.14	37.18
B3LYP[a]	−18.08	3.93	−2.89	11.73	−15.38	−0.89	−1.66	27.48
CAM-B3LYP	−16.60	5.00	−2.95	11.56	−13.00	−0.80	−0.51	31.33
M06-2X	8.20	5.72	12.72	11.85	5.62	5.21	8.20	35.41
M06	6.53	2.64	31.24	16.56	17.94	1.44	19.73	33.87
wB97XD	−6.87	−5.19	8.18	14.80	−0.46	1.55	10.80	35.74
PBE-D3BJ	5.78	4.13	22.80	16.66	9.65	−1.84	19.69	32.07
B2PLYP	−7.86	4.17	5.74	12.94	0.56	−1.92	8.63	31.20
B2PLYPD	−1.77	6.31	16.80	20.03	9.08	2.34	20.57	37.53
B2PLYPD3	3.15	6.12	18.02	17.84	11.32	2.18	19.31	35.38
wPW2PLYP	−8.64	4.53	5.05	13.29	−1.13	−1.20	7.69	31.72
wPW2PLYPD	−4.21	6.08	13.09	18.45	5.07	1.87	16.37	36.32
DSDPBEP86	6.82	4.95	21.30	17.53	18.52	0.71	22.65	36.56
PBE0DH	2.32	5.45	15.97	16.78	3.05	0.09	14.23	35.30
PBEQIDH	5.09	5.39	18.22	16.96	12.06	−0.47	18.75	36.71

[a]Data taken from ref 29.

https://doi.org/10.1021/acsomega.1c02016
ACS Omega 2021, 6, 16612−16622

Table 2. $\Delta\Delta G$ Values Calculated as Differences between the Calculated ΔG with DFT Functionals and MP2 ΔG Values, in kcal/mol. Average Values of Calculated Differences and Standard Deviations Are Also Given in kcal/mol[a]

	^{5}Ti		^{7}Cr		^{3}Ni		^{1}Zn		
	$\Delta\Delta E_{S\text{-}E}$	$\Delta\Delta E_{TS}$	$\Delta\Delta E_{S\text{-}E}$	$\Delta\Delta E_{TS}$	$\Delta\Delta E_{S\text{-}E}$	$\Delta\Delta E_{TS}$	$\Delta\Delta E_{S\text{-}E}$	$\Delta\Delta E_{TS}$	Ave ± σ
B3LYP[a]	−23.66	−1.45	−22.69	−4.84	−24.12	1.12	−28.80	−9.70	14.56 ± 10.67
CAM-B3LYP	−22.19	−0.39	−22.75	−5.01	−21.74	1.31	−27.65	−5.85	13.36 ± 10.49
M06-2X	2.62	0.34	−7.08	−4.72	−3.12	7.32	−18.84	−1.77	5.74 ± 5.80
M06	0.95	−2.74	11.44	1.99	9.19	3.54	−7.41	−3.30	5.07 ± 3.54
wB97XD	−12.45	−0.19	−11.62	−1.77	−9.20	3.65	−16.34	−1.44	5.08 ± 5.49
PBE-D3BJ	0.20	−1.25	3.00	0.09	0.91	0.26	−7.45	−5.11	1.17 ± 3.20
B2PLYP	−13.44	−1.21	−14.06	−3.63	−8.18	0.18	−18.51	−5.98	8.15 ± 6.20
B2PLYPD	−7.35	0.93	−3.00	3.46	0.33	4.44	−6.57	0.35	3.30 ± 2.54
B2PLYPD3	−2.43	0.74	−1.78	1.27	2.58	4.28	−7.83	−1.80	2.84 ± 2.13
wPW2PLYP	−14.22	−0.85	−14.75	−3.28	−9.87	0.90	−19.45	−5.46	8.60 ± 6.58
wPW2PLYPD	−9.79	0.70	−6.71	1.88	−3.67	3.97	−10.77	−0.86	4.79 ± 3.66
DSDPBEP86	1.24	−0.43	1.50	0.96	9.78	2.81	−4.49	−0.62	2.73 ± 2.95
PBE0DH	−3.26	0.07	−3.83	0.21	−5.69	2.19	−12.91	−1.88	3.76 ± 3.87
PBEQIDH	−0.49	0.01	−1.58	0.39	3.32	1.63	−8.39	−0.47	2.04 ± 2.60

[a]Data taken from ref 29.

in the assessment of the quality of the MP2 reference. Finally, to analyze the noncovalent interactions, we have used the NCIplot4 software.[54−56]

Ab Initio Born−Oppenheimer molecular dynamics (BO-MD) simulations were performed to additionally explore the thermal stability of selected TM$(ZnS)_{12}$. The PBE-D3BJ functional was used as described above, combined with a DZP quality basis set and the RI formalism with the corresponding auxiliary basis sets.[57−59] The temperature was set to 300 K using the Nosé−Hoover thermostat. The simulation was run for 10000 steps, with a time step of 300 au (7.26 fs) resulting in simulation times as long as 300000 au (7.26 ps). The TURBOMOLE package[60] was used to carry out all these simulations.

3. RESULTS AND DISCUSSION

3.1. Benchmark of the Density Functional (Method Calibration). Second-order Møller−Plesset perturbation theory, MP2, is the computationally cheapest post-Hartree−Fock method that accurately describes the van der Waals interactions, with limitations, and is free of electron self-interaction error. This method, however, is still computationally very demanding, especially for geometry optimizations and frequency calculations. For this reason, we have tested several DFT functionals (B3LYP, CAM-B3LYP, M06, M06-2X, wB97XD, PBE-D3BJ, B2PLYP, mPW2PLYP, B2PLYPD, mPW2PLYPD, B2PLYPD3, DSDPBEP86, PBE0DH, and PBEQIDH) against this method, in order to assess the quality of the MP2 value as reference and to identify the level of theory that provides a balance between accuracy and computational cost, in order to use this functional for the rest of the calculations.

In our previous work, the (ZnS) nanoclusters with a first-row TM located inside the cavity (*ENDO*) and at the surface of the cavity (*SURFACE*), along with the transition states connecting both isomers, were characterized using the B3LYP functional[29] (see Figure 1). Now single-point calculations were performed on these TM$(ZnS)_{12}$ structures with MP2 and several DFT functionals. In Table 1 the electronic energy difference between *SURFACE* and *ENDO* isomers ($\Delta E_{S\text{-}E} = E_{Surf} - E_{Endo}$) as well as the energy difference between *ENDO* and transition-state structures ($\Delta E_{TS} = E_{TS} - E_{Endo}$) is shown for ^{5}Ti, ^{7}Cr, ^{3}Ni, and ^{1}Zn doped $(ZnS)_{12}$. These spin states and transition metals have been chosen as representative for early, middle, and late first-row TMs with high and low spins.

According to the results obtained with the B3LYP functional[29] in Table 1, all *SURFACE* structures are more stable than the corresponding *ENDO* ones. Similar results are obtained with CAM-B3YP, and according to wB97XD for ^{5}Ti and ^{3}Ni, the *ENDO* compounds are the most stable. On the contrary, MP2 data given in Table 1 shows that in all the cases *ENDO* compounds are more stable than the corresponding *SURFACE* structures. Remarkable are the calculated differences of ca. 20 and 27 kcal/mol for ^{7}Cr and ^{1}Zn, respectively. Hence, the consideration of dispersion interactions appears to be crucial in stabilizing the *ENDO* structures, where the TM is located inside the $(ZnS)_{12}$ cavity. The results obtained with the remaining DFT functionals support qualitatively the conclusion obtained with MP2 and show the importance of dispersion. Note that in some cases negative values are calculated for ΔE_{TS}. These energetic values are obtained by means of single-point calculations using geometries optimized in ref 29 and not at geometries optimized at each level of theory. In addition, thermal and entropic corrections are not considered at this stage. These two facts may explain the negative values calculated for ΔE_{TS}.

Table 2 contains the $\Delta\Delta E$ values calculated as the differences between the computed ΔE values with DFT functionals and with MP2 and the calculated difference averages and standard deviations. The average difference of wB97XD with respect to MP2 is similar to those calculated for M06 and M06-2X (around 5 kcal/mol), but unlike the first one, the last two correctly predict the endohedral structures as the most stable ones for all the cases studied. Double-hybrid functionals including empirical dispersion terms are slightly closer to MP2, with average differences around 2−3 kcal/mol, predicting the same isomer as the most stable one. PBE-D3BJ is the method that provides the closest results to MP2. In general, compared to DFT functionals, MP2 energetics favor the endohedral structure by approximately an extra 3−5 kcal/mol, which can be attributed to the known overestimation of dispersion interactions. Considering these results, and because the computational cost of double-hybrid functionals is that of MP2 and not DFT, and the RI formalism in TURBOMOLE is

https://doi.org/10.1021/acsomega.1c02016
ACS Omega 2021, 6, 16612−16622

supported only for pure functionals, the PBE-D3BJ method is the chosen one to be used hereafter. In this way, Born−Oppenheimer molecular dynamics calculations will be affordable.

3.2. Full Characterization of (^{5}Ti, ^{7}Cr, ^{3}Ni, ^{1}Zn)@$(ZnS)_{12}$ Structures. Previously first-row TM doped ZnS nanoclusters were studied, and it was concluded that only Zn would remain enclosed inside the cluster, whereas for the rest of the TMs the preferred position would be at the surface.[29] Nevertheless, as shown in the previous section, dispersion interactions could change this in favor of endohedral doping. To unveil this question *ENDO* and *SURFACE* compounds, along with the transition states connecting both structures, have been fully optimized with the PBE-D3BJ functional for (^{5}Ti, ^{7}Cr, ^{3}Ni, ^{1}Zn)@$(ZnS)_{12}$. Since frequency calculations are carried out in these characterizations, hereafter Gibbs free energies will be considered.

In Table 3 the geometrical and energetic data of such structures are shown. For the *ENDO* compounds, Zn and Cr atoms are located at the center of the cavity, while Ti and Ni are moved from the center, breaking the symmetry of the system.

Table 3. Distance of the TM with the Geometrical Center of the $(ZnS)_{12}$ Cage, *R*, in Å and the Symmetry Group of the Calculated Structures and $\Delta G_{S\text{-}E}$ and ΔG_{TS} in kcal/mol

	ENDO		*SURFACE*		
Metal	*R*	Symm	Symm	$\Delta G_{S\text{-}E}$	ΔG_{TS}
^{5}Ti	0.91	C_1	C_1	−5.12	−1.78
^{7}Cr	0.00	D_{2h}	C_1	16.28	18.61
^{3}Ni	1.01	C_1	C_1	−0.58	3.73
^{1}Zn	0.00	D_{2h}	C_1	19.83	35.34

Our results predict that the *ENDO* structures are thermodynamically more stable than the corresponding *SURFACE* ones for ^{7}Cr and ^{1}Zn doped clusters. Similarly, these two metals are the ones that exhibit the largest energy barriers for the *ENDO*-to-*SURFACE* isomerization reaction. We would like to point out that according to the B3LYP functional, the *SURFACE* structures are more stable than the corresponding *ENDO*.[26] These results suggest that the van der Waals forces are responsible for the stabilization of the TM at the center of the $(ZnS)_{12}$ and they are indeed fundamental for the correct description of these systems. In fact, ^{7}Cr and ^{1}Zn atoms are located at the center of the cluster, with no covalent bonds between the guest and the host but only second-order weak interactions. In the case of ^{5}Ti and ^{3}Ni doped clusters, the *SURFACE* and *ENDO* structures are now closer in energy, with energy differences within 5 kcal/mol. For ^{5}Ti doped $(ZnS)_{12}$, the computed energy barrier for the *ENDO*-to-*SURFACE* isomerization is −1.78 kcal/mol. Notice that this negative number suggests that this is a barrierless process, and hence only the surface structure would be obtained experimentally.

With the aim of verifying the relevance of dispersion forces in *ENDO* compounds, Zn, Cr, Ni, and Ti doped *ENDO* and *SURFACE* structures are analyzed using the noncovalent interaction index (NCI), that is a visualization tool based on the density and the reduced density gradient (RDG). The NCI allows identifying noncovalent interactions in real space, characterized by regions with low RDG and density values. The NCI can detect both attractive and repulsive interactions. The first are represented by a negative sign of the Hessian's second eigenvalue (λ_2), while positive values indicate a repulsive interaction. van der Waals or dispersion interactions correspond to regions where $\lambda_2 \approx 0$.

Figure 2 represents the regions of space where these interactions are relevant. Blue areas correspond to strong, attractive interactions, green to dispersion interactions, and red to strong repulsive interactions. As shown in Figure 2, dispersion interactions are more relevant in the *ENDO* conformation than in the *SURFACE* one. That indicates the relevancy of these interactions to account for energy differences between the two conformers properly. For Cr and Zn, the *ENDO* conformers are symmetric with the metal located at the center of the cage in both cases. Inspection of Figure 2 indicates that in these cases, the van der Waals region is fully symmetric around the metal, stabilizing the position of the metals at the center of the cage. On the other hand, Ti and Ni in the *ENDO* conformers are not symmetric, and the metals are located closer to the surface of the cage. Those displacements break the symmetry of the van der Waals areas, being in these cases less relevant in regions with closer TM−ZnS distances. This qualitative analysis reveals the importance of dispersions interactions to calculate conformer stabilization energies for different TMs.

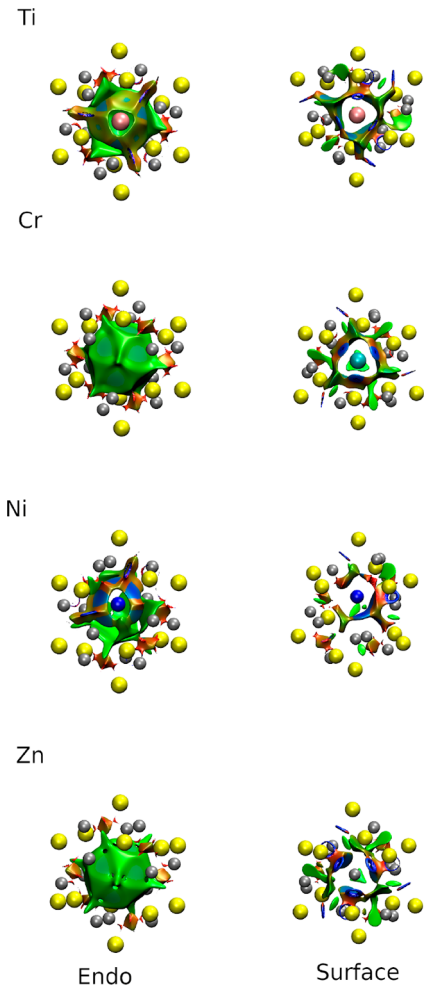

Figure 2. NCI analysis of TM doped $(ZnS)_{12}$ nanoclusters. RDG isosurface with an isovalue of 0.3 au.

https://doi.org/10.1021/acsomega.1c02016
ACS Omega 2021, 6, 16612−16622

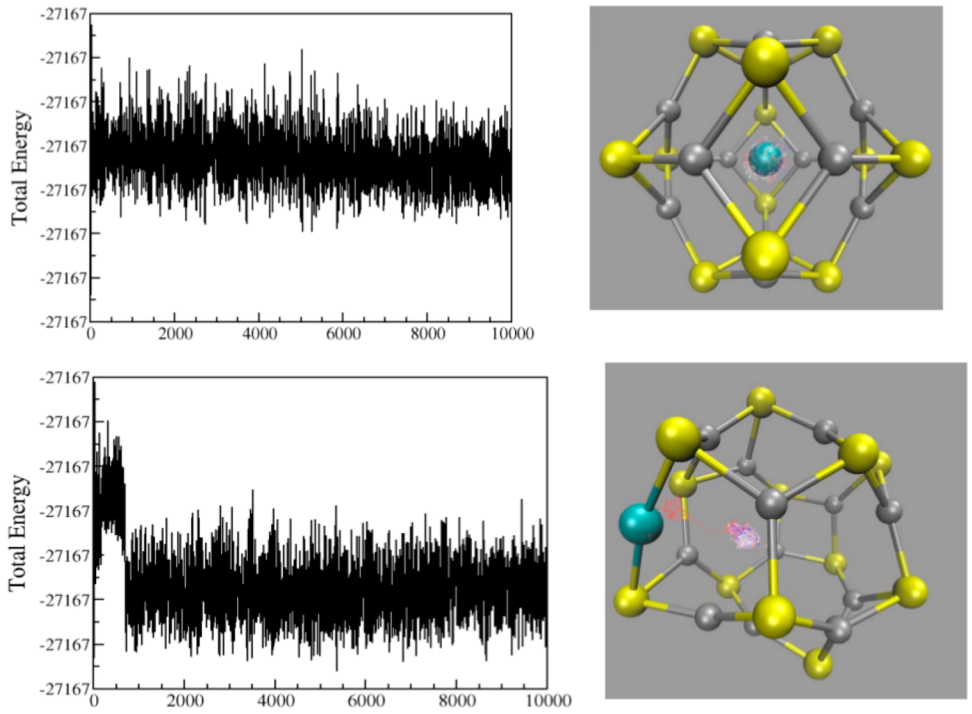

Figure 3. Quantum molecular dynamics results for $^{7}Cr(ZnS)_{12}$ structures. Total energies and the trajectory of the ^{7}Cr along the simulation time (top) for the *ENDO* structure and (bottom) for the *SURFACE* structure. On the left, total energies are depicted vs simulation steps. Each step is 300 au.

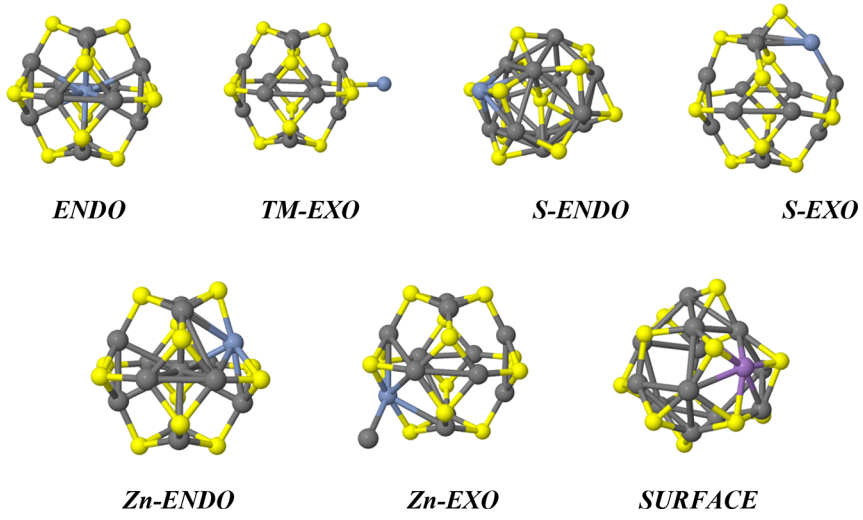

Figure 4. Examples of the seven structure family isomers detected in the MD simulations.

It is important to note that those transition metals that prefer to be located at the center of the cage, ^{7}Cr and ^{1}Zn, have half-full or full 4s3d shells. Specifically ^{7}Cr has $4s^{1}3d^{5}$ electronic configuration and ^{1}Zn $4s^{2}3d^{10}$. Hence, the spherical shape of the electronic density in these atoms may be determinant for enhancing the stability of the *ENDO* compounds. Having all this in mind, quantum molecular dynamics (QMD) simulations have been carried out for the *ENDO* and *SURFACE* compounds of the four metals (^{7}Cr, ^{1}Zn, ^{5}Ti, and ^{3}Ni), along with selected cases of isoelectronic anionic and cationic TMs that possess spherical electronic structures (see the Supporting Information for details). In addition to the thermal stability, these simulations may also provide the existence of other isomers different from the *ENDO* and *SURFACE* considered until now, yielding a deeper knowledge of the configurational space of these compounds. The obtained results are detailed below.

3.3. Molecular Dynamics Simulations at 300 K.

According to PBE-D3BJ geometry optimizations, ^{7}Cr prefers to be at the center of the cavity and ^{5}Ti at its surface. Born–Oppenheimer MD simulations were performed for both the *ENDO* and the *SURFACE* $^{7}Cr(ZnS)_{12}$ and $^{5}Ti(ZnS)_{12}$ structures, as shown in Figure 3. For the Cr doped *ENDO* structure it was found that the structure remains intact after 7.26 ps. Conversely, for the *SURFACE* conformer, it was found that after around 500 time steps (0.36 ps), the dopant atom moves from the surface of the cluster to the center of the cavity. This reconstruction from the *SURFACE* to the *ENDO*

https://doi.org/10.1021/acsomega.1c02016
ACS Omega 2021, 6, 16612−16622

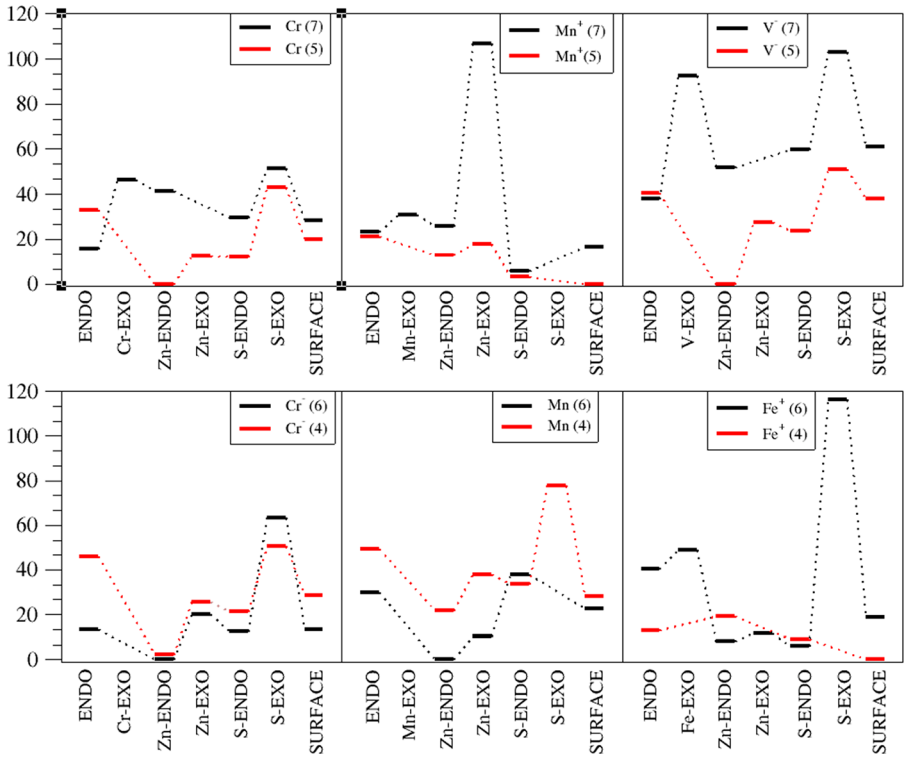

Figure 5. Energy profiles of all the TM doped $(ZnS)_{12}$, in which the TM has either $4s^1d^5$ (above) or $4s^2d^5$ (below) electronic structure.

isomers is accompanied by a sudden energy decrease. Therefore, not only is the *SURFACE* compound thermodynamically less stable than the *ENDO* isomer, but it is not thermally stable and it will spontaneously rearrange into the *ENDO* structure at room temperature. This fact is especially relevant for the synthesis of this kind of compound, where the TM would be very likely incorporated into the cluster afterward. For $^5Ti(ZnS)_{12}$, however, the *SURFACE* structure is predicted to be more stable than the corresponding *ENDO*. MD simulations show that the latter is indeed not thermally stable, since Ti would move from the center to the surface, accompanied by an energy decrease, as observed in Figure S1 of the Supporting Information.

In addition to these simulations, Born−Oppenheimer molecular dynamics of selected isoelectronic TM-$Zn_{12}S_{12}$ *ENDO* and *SURFACE* structures were carried out, namely: $4s^13d^5$ (Cr, V^-), $4s^23d^5$ (Mn, Cr^-), $4s^13d^{10}$ (Cu, Ni^-), and $4s^23d^{10}$ (Zn). The most relevant finding in these cases was that the *ENDO* structure is stable for ^{7}Cr, ^{2}Cu, and ^{1}Zn, while in other cases the $TM(ZnS)_{12}$ clusters visited several local minima during the simulation time. Such isomers might be classified into families: *ENDO* structures with different atoms inside the cavity (TM, Zn, or S), *EXO* structures with different atoms outside the cage structure (TM, Zn or S), and the *SURFACE* structure. As it can be observed, from the representative structures of such families depicted in Figure 4, the potential energy surface of $TM(ZnS)_{12}$ is rich in low-lying isomers that might be reachable at room temperature.

3.4. Isomer Stability. According to MD and the geometry optimizations in previous sections, metals with more spherical electronic densities, namely those with half-full or full 4s3d electronic structure, are the best candidates to form stable endohedrally doped ZnS clusters. For this reason, we decided to perform an exhaustive search of the potential energy surface of these systems, by characterizing (geometrical optimization) each of the local minima found in the MD simulations, with the following TMs doped $(ZnS)_{12}$ clusters: $4s^13d^5$ (Cr, Mn^+, V^-), $4s^23d^5$ (Mn, Fe^+, Cr^-), $4s^13d^{10}$ (Cu, Zn^+, Ni^-), and $4s^23d^{10}$ (Zn, Cu^-). To have an even broader view of all the electronic and structural possibilities of such compounds, we considered the low- and high-spin states of the TMs.

3.4.1. $4s^13d^5$ and $4s^23d^5$ Nanoclusters. In this case, all the valence electrons in the 3d atomic orbitals, AOs, are unpaired, with a multiplicity $2S + 1 = 7$ or 6. The corresponding low-lying spin state, with two of the 3d electrons paired and $2S + 1 = 5$ or 4, was explored too. The energy profiles in Figure 5 show that low-spin structures are in general thermodynamically more stable in $4s^13d^5$ than in $4s^23d^5$. Indeed in the former, going from high-spin to low-spin leads to only one pair of 3d paired electrons, but in the latter, it leads to two pairs of 3d paired electrons. The most stable isomers for each case are depicted in Figure 6. The *ENDO* isomer is the global minima for ^{7}Cr and $^7V^-$. This result correlates well with the MD simulations shown above and holds them promising for functionalized materials with well-defined magnetic properties. In both $^7Cr@(ZnS)_{12}$ and $^7V^-@(ZnS)_{12}$ all the valence orbitals are singly occupied and symmetrically distributed in the space, so the interaction between the metal and the cluster is equivalent in all directions confining the TM in the cavity center. Thus, dispersion is key for the stabilization of these structures. However, when two electrons are paired in ^{5}Cr and $^5V^-$, the symmetry is broken and the system is destabilized.

When the TM is not at the center of the cage, it forms covalent bonds with the closest Zn and S and, as a result, other conformers are thermodynamically stabilized. Particularly interesting is the case of *Zn-ENDO*, where the TM and one of the Zn atoms of the cluster switched positions, leading to the encapsulation of that Zn. We found that this is the most

https://doi.org/10.1021/acsomega.1c02016
ACS Omega 2021, 6, 16612−16622

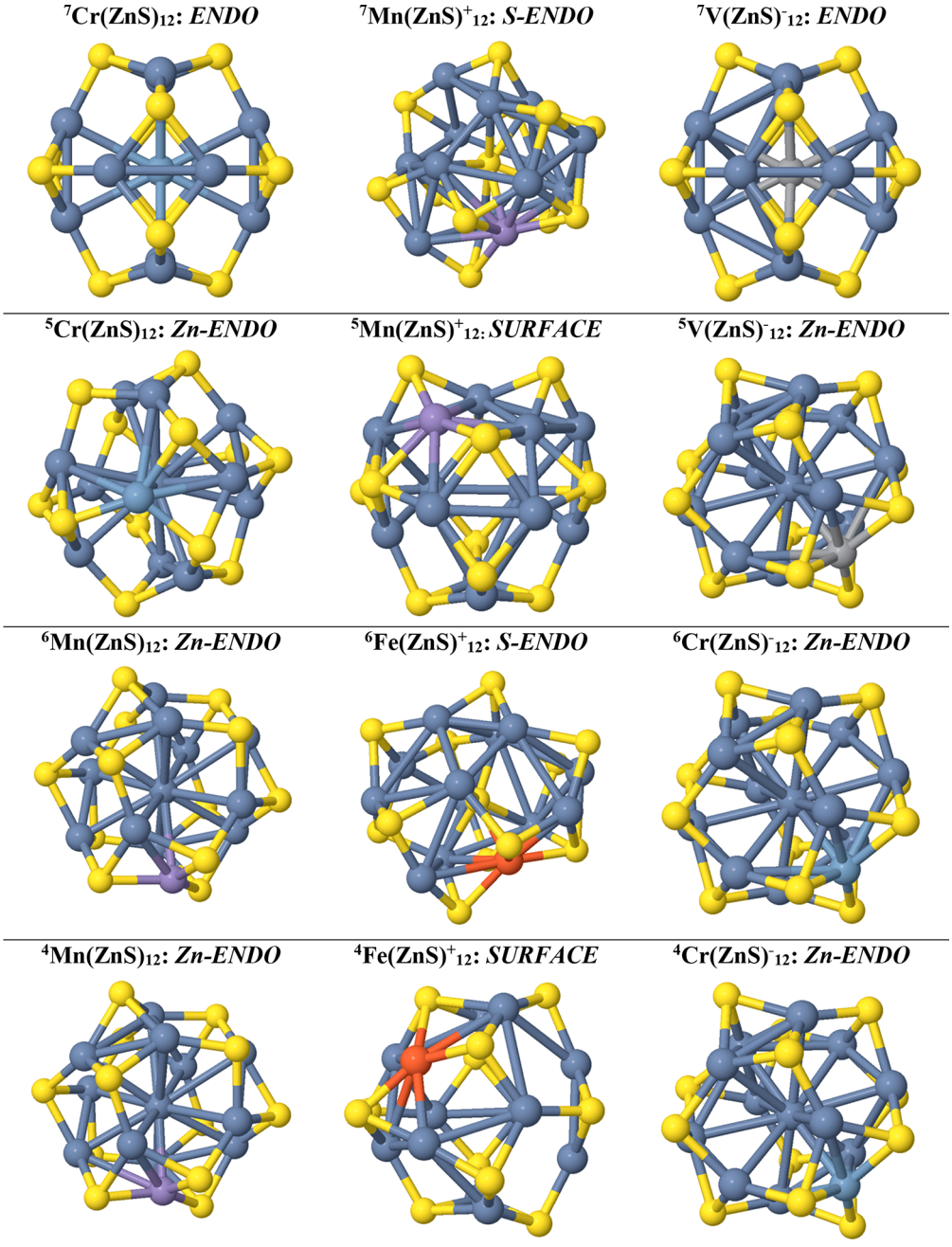

Figure 6. Most stable high- and low-spin structures for all the TM doped $(ZnS)_{12}$, in which the TMs have either $4s^1d^5$ or $4s^2d^5$ electronic structure.

thermodynamically stable isomer in most cases. For ^{5}Cr, ^{4} Mn, and ^{6} Mn, the dopant atom substitutes one Zn atom (while that Zn atom sits at the center of the cluster) retaining the original shape of the cluster. Considering that Zn has a full 3d shell, this scenario agrees with the hypothesis that the endohedral structures are stable when the atom inside the cavity has half-full or full 4s3d shells, stabilized through van der Waals forces.

For the anionic $^{5}V^{-}$, $^{4}Cr^{-}$, and $^{6}Cr^{-}$ doped clusters, the most stable structure is *Zn-ENDO* too. Nevertheless, the resulting structures are significantly distorted, due to the displacement of the anion from the surface toward the encapsulated Zn atom. Because Zn has a partial positive charge, such distortion can be seen as a consequence of the electrostatic attractive interaction between the anionic metal and the Zn atom lying inside the cluster.

In the cationic clusters, conversely, the most thermodynamically stable structures are the ones in which the bonding between the dopant and the S atoms holding partial negative charges is maximized. Regarding the high-spin state, Mn^{+} and Fe^{+} are stabilized the most in the *S-ENDO* structure. Here, one S atom is encapsulated inside the cluster, and the dopants move inward, in order to bond it, resulting in a very distorted and shrunk geometry. For low-spin states, the *SURFACE* structure is the most thermodynamically stable. In this case, the cationic metal bonds to several S atoms in the surface of the cage, leading to a more expanded shape. Therefore, the electrostatic interactions appear to be the reason for the preference of those isomers. Indeed, the structures that are stabilized with Mn^{+} and Fe^{+} are the ones in which the interaction between the TM^{+} and Zn (with a partial positive charge) is minimized and that between the TM^{+} and S (with a

https://doi.org/10.1021/acsomega.1c02016
ACS Omega 2021, 6, 16612−16622

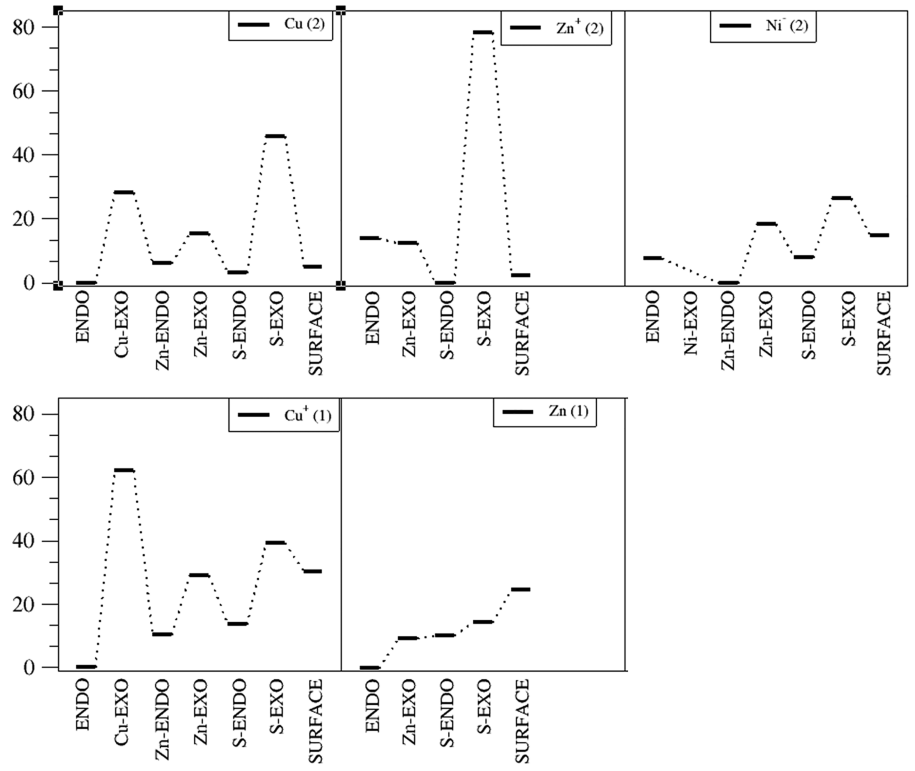

Figure 7. Energy profiles of all the TM doped $(ZnS)_{12}$, in which the TMs have either $4s^1d^{10}$ (top) or $4s^2d^{10}$ (bottom) electronic structure.

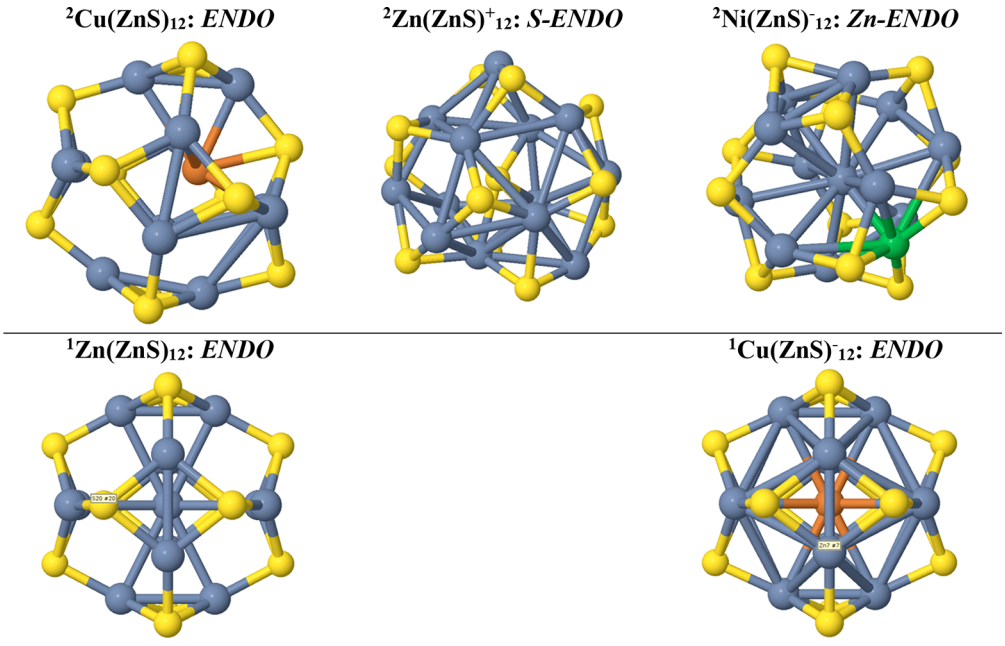

Figure 8. Most stable high- and low-spin structures for all the considered TM doped $(ZnS)_{12}$, in which the TMs have either $4s^1d^{10}$ or $4s^2d^{10}$ electronic structure.

partial negative charge) is maximized. For this same reason, *Zn-EXO* and *S-EXO* structures are unstable or very high in energy for Mn^+ and Fe^+ cationic metals. Finally, for Mn^+, we found for the first time that *ENDO* is more thermodynamically stable for $^5Mn^+$ than for $^7Mn^+$, although the energy difference between them is small. This energy difference is larger in the case of Fe^+.

3.4.2. $4s^13d^{10}$ and $4s^23d^{10}$ Nanoclusters. The group $4s^13d^{10}$ has its 3d AOs fully occupied. We would like to point out that the higher multiplicity is achieved by exciting one 3d electron to the 4p AO, and we anticipate that the high-spin-state compounds are not energetically competitive in any case. Therefore, we only considered here the low spin states. Note also that for Zn doped $(ZnS)_{12}$ there exist fewer isomers, since the *ENDO* and *Zn-ENDO*, as well as the *TM-EXO* and *Zn-EXO* conformers, are equivalent.

The energy profiles for this group of TM doped $(ZnS)_{12}$ are shown in Figure 7. The most stable isomers for each case are

https://doi.org/10.1021/acsomega.1c02016
ACS Omega 2021, 6, 16612−16622

depicted in Figure 8. For ^{2}Cu the most thermodynamically stable isomer is the endohedral compound, *ENDO*, stabilized by van der Waals interactions. Although it is very close in energy to several isomers, such as the *SURFACE* one, the most stable position for $^{1}Cu^{+}$ and ^{1}Zn dopants is the center of the cage as well. Unfortunately, these metals have no unpaired electrons ($4s^{1}3d^{10}$), and thus they will not lead to materials with magnetic properties.

The most thermodynamically stable conformer for $^{2}Ni^{-}$ is *Zn-ENDO*, similar to most of the anionic compounds shown previously. Led by electrostatic forces, Ni^{-} moves into the cage to bond the encapsulated Zn atom, distorting the cluster. Note that this structure is very close in energy to *ENDO*. For Zn^{+}, as was found for the other cationic species considered above, the most stable structure is *S-ENDO*, where the cation is able to maximize the number of bonds with the electronegative S atoms.

4. CONCLUSIONS

The endohedrally doped II−VI semiconductor nanomaterials with TMs present a very important feature in dealing with the magnetic properties of 2D or 3D of such cluster-assembled materials, as the TM−TM distance is fixed. In fact, the magnetic properties of these compounds have been found to be connected with the TM−TM distances in related materials. Previously, first- and second-row TM doped ZnS nanoclusters were studied. Two different structures were considered for each case, i.e., endohedral (where the TM is located at the center of the cluster) and exohedral structures (where the TM is at the surface of the cluster). The main conclusion of the work was that generally the TM atoms prefer to be located at the surface of the ZnS clusters and the lifetimes of the endohedral structures were very small. In these studies, however, dispersion interactions were not considered. Here, after carefully choosing the adequate level of theory, we show that the dispersion interactions between the dopant TM and the ZnS nanocluster play a key role in stabilizing some of the endohedral compounds. Additionally, a complete family of TM doped ZnS nanoclusters is explored using *ab initio* molecular dynamics simulations and local minima optimizations. This study could guide the experimental synthesis of such compounds and help obtain a holistic picture of the interaction between TM and II−VI nanomaterials.

When the dopant atom is charged, the electrostatic forces will be dominant over the dispersion forces. Consequently, for positively charged dopants, the endohedral compounds are thermodynamically less stable than other isomers, due to the electrostatic repulsion between the dopant and the Zn atoms of the cage that are pointing inward the cavity. However, we found that Cr, V^{-}, and Cu are the perfect candidates to obtain endohedrally doped ZnS compounds and hold them promising for functionalized materials with well-defined magnetic properties. First, the endohedral structures are the most stable ones for these candidates; second, they are capable of giving magnetic properties to the semiconducting clusters due to their unpaired electrons.

ASSOCIATED CONTENT

Supporting Information

The Supporting Information is available free of charge at https://pubs.acs.org/doi/10.1021/acsomega.1c02016.

Ab initio molecular dynamics simulations, Gibbs free energies of optimized structures, relative Gibbs free energies with respect to the most stable isomer, and cartesian coordinates of optimized structures (PDF)

AUTHOR INFORMATION

Corresponding Author

Elisa Jimenez-Izal − *Polimero eta Material Aurreratuak: Fisika, Kimika eta Teknologia Saila, Kimika Fakultatea, Euskal Herriko Unibertsitatea (UPV/EHU) and Donostia International Physics Center (DIPC), 20018 Donostia, Euskadi, Spain; IKERBASQUE, Basque Foundation for Science, 20018 Bilbao, Euskadi, Spain;* orcid.org/0000-0003-1127-2100; Email: elisa.jimenez@ehu.es

Authors

Iker Ortiz de Luzuriaga − *CIC nanoGUNE BRTA, E-20018 Donostia, Euskadi, Spain*

Eloy Ramos-Cordoba − *Polimero eta Material Aurreratuak: Fisika, Kimika eta Teknologia Saila, Kimika Fakultatea, Euskal Herriko Unibertsitatea (UPV/EHU) and Donostia International Physics Center (DIPC), 20018 Donostia, Euskadi, Spain;* orcid.org/0000-0002-6558-7821

Jon M. Matxain − *Polimero eta Material Aurreratuak: Fisika, Kimika eta Teknologia Saila, Kimika Fakultatea, Euskal Herriko Unibertsitatea (UPV/EHU) and Donostia International Physics Center (DIPC), 20018 Donostia, Euskadi, Spain;* orcid.org/0000-0002-6342-0649

Complete contact information is available at: https://pubs.acs.org/10.1021/acsomega.1c02016

Notes

The authors declare no competing financial interest.

The data that support the findings of this study are available from the corresponding author upon reasonable request.

ACKNOWLEDGMENTS

Financial support comes from Eusko Jaurlaritza through project IT1254-19. The authors are thankful for technical and human support provided by SGIker (UPV/EHU, ERDF, EU). E.J.I. acknowledges the support of the Ikerbasque Fellowship. E.R.C. acknowledges funding from the Juan de la Cierva program IJCI-2017-34658.

REFERENCES

(1) Singh, R.; Basu, S.; Pal, B. Ag^{+} and Cu^{2+} Doped CdS Nanorods with Tunable Band Structure and Superior Photocatalytic Activity Under Sunlight. *Mater. Res. Bull.* **2017**, *94*, 279−286.

(2) Arango, A. C.; Oertel, D. C.; Xu, Y.; Bawendi, M. G.; Bulovic, V. Heterojunction Photovoltaics Using Printed Colloidal Quantum Dots as a Photosensitive Layer. *Nano Lett.* **2009**, *9*, 860−863.

(3) Horoz, S.; Dai, Q.; Maloney, F. S.; Yakami, B.; Pikal, J. M.; Zhang, X.; Wang, J.; Wang, W.; Tang, J. Absorption Induced by Mn Doping of ZnS for Improved Sensitized Quantum-dot Solar Cells. *Phys. Rev. Appl.* **2015**, *3*, 024011−024017.

(4) Park, W.; King, J. S.; Neff, C. W.; Liddell, C.; Summers, C. J. ZnS-Based Photonic Crystals. *Phys. Status Solidi B* **2002**, *229*, 949−960.

(5) Rafea, M. A.; Farag, A. A. M.; Roushdy, N. Structural and Optical Characteristics of Nano-Sized Structure of Zn0.5Cd0.5S Thin Films Prepared by Dip-Coating Method. *J. Alloys Compd.* **2009**, *485*, 660−666.

(6) Infante, I.; Azpiroz, J. M.; Blanco, N. G.; Salassa, L. Quantum Dot Photoactivation of Pt(IV) Anticancer Agents: Evidence of an

Electron Transfer Mechanism Driven by Electronic Coupling. *J. Phys. Chem. C* **2014**, *118*, 8712−8721.
(7) Ramasamy, V.; Praba, K.; Murugadoss, G. Synthesis and Study of Optical Properties of Transition Metals Doped ZnS Nanoparticles. *Spectrochim. Acta, Part A* **2012**, *96*, 963−971.
(8) Godlewski, M.; Yatsunenko, S.; Khachapuridze, A.; Ivanov, V. Yu.; Gołacki, Z.; Karczewski, G.; Bergman, P. J.; Klar, P. J.; Heimbrodt, W.; Phillips, M. R. J. Mechanism of Intra-shell Recombination of Transition Metal and Rare Earth Ions in Nanostructures of II-VI Compounds. *J. Alloys Compd.* **2004**, *380*, 45−49.
(9) Poggio, S.; Wang, B.; Gibson, U. J.; BelBruno, J. J. Properties of Transition Metal Substituted Zinc Sulfide Hexamers and Dodecamers. *Phys. Chem. Chem. Phys.* **2015**, *17*, 14208−14214.
(10) Dhara, A.; Sain, S.; Das, S.; Pradhan, S. K. Microstructure, Optical and Electrical Characterizations of Mn Doped ZnS Nanocrystals Synthesized by Mechanical Alloying. *Mater. Res. Bull.* **2018**, *97*, 169−175.
(11) Jimenez-Izal, E.; Matxain, J. M.; Piris, M.; Ugalde, J. M. Second-Row Transition-Metal Doping of (Zn_iS_i), i = 12, 16 Nanoclusters: Structural and Magnetic Properties. *Computation* **2013**, *1*, 31−45.
(12) Archer, P. I.; Santangelo, S. A.; Gamelin, D. R. Inorganic Cluster Synthesis of TM^{2+}-Doped Quantum Dots (Cd/Se, CdS, CdSe/CdS): Physical Property Dependence on Dopant Locale. *J. Am. Chem. Soc.* **2007**, *129*, 9808−9818.
(13) Poggio, S.; King, J.; BelBruno, J. J. Properties of Transition Metal Doped Cadmium Sulfide Hexamers and Dodecamers. *Chem. Phys. Lett.* **2015**, *640*, 106−111.
(14) Li, Y. Q.; Zapien, J. A.; Shan, Y. Y.; Liu, Y. K.; Lee, S. T. Manganese Doping and Optical Properties of ZnS Nanorribons by Postannealing. *Appl. Phys. Lett.* **2006**, *88*, 013115−013117.
(15) Andriotis, A. N.; Menon, M. Universal Features Underlying the Magnetism in Diluted Magnetic Semiconductors. *J. Phys.: Condens. Matter* **2018**, *30*, 135803.
(16) Hu, Y.; Ji, C.; Wang, X.; Huo, J.; Liu, Q.; Song, Y. The Structural, Magnetic and Optical Properties of $TM_n@(ZnO)_{42}$ (TM = Fe, Co and Ni) Hetero-nanostructure. *Sci. Rep.* **2017**, *7*, 16485−16495.
(17) Meulenberg, R. W.; van Buuren, T.; Hanif, K. M.; Willey, T. M.; Strouse, G. F.; Terminello, L. J. Structure and Composition of Cu-Doped CdSe Nanocrystals Using Soft X-ray Absorption Spectroscopy. *Nano Lett.* **2004**, *4*, 2277−2285.
(18) Chandramohan, S.; Kanjilal, A.; Tripathi, J. K.; Sarangi, S. N.; Sathyamoorthy, R.; Som, T. Structural and Optical Properties of Mn-doped CdS Thin Films Prepared by Ion Implantation. *J. Appl. Phys.* **2009**, *105*, 123507−123510.
(19) Yang, F.; Yan, N.-N.; Huang, S.; Sun, Q.; Zhang, L.-Z.; Yu, Y. Zn-Doped CdS Nanoarchitectures Prepared by Hydrothermal Synthesis: Mechanism for Enhanced Photocatalytic Activity and Stability Under Visible Light. *J. Phys. Chem. C* **2012**, *116*, 9078−9084.
(20) Zhao, J.; Du, Q.; Zhou, S.; Kumar, V. Endohedrally Doped Cage Clusters. *Chem. Rev.* **2020**, *120*, 9021−9163.
(21) Liu, H.; Wang, S.; Zhou, G.; Wu, J.; Duan, W. Structural, Electronic, and Magnetic Properties of Manganese-Doped $Zn_{12}O_{12}$ Clusters: A First-Principles Study. *J. Chem. Phys.* **2006**, *124*, 174705−174712.
(22) Ganguli, N.; Dasgupta, I.; Sanyal, B. Electronic Structure and Magnetism of Transition Metal Doped $Zn_{12}O_{12}$ clusters: Role of Defects. *J. Appl. Phys.* **2010**, *108*, 123911−123919.
(23) Yong, Y.; Wang, Z.; Liu, K.; Song, B.; He, P. Structures, Stabilities, and Magnetic Properties of Cu-Doped Zn_nO_n (n = 3, 9, 12) Clusters: A Theoretical Study. *Comput. Theor. Chem.* **2012**, *989*, 90−96.
(24) Chen, H.; Shi, D.; Qi, J.; Wang, B. First-Principles Study on the Structure, Electronic, and Magnetic Properties of Mn-doped $(ZnS)_{12}$ Clusters. *Phys. E* **2010**, *43*, 117−124.
(25) Li, Z.; Zhao, Z.; Xue, G.-w.; Wu, J.; Shen, X. Theoretical Prediction of the Configurations, Electronic and Magnetic Properties of the Transition-Metal@$Zn_{12}S_{12}$ Clusters. *Mater. Chem. Phys.* **2021**, *258*, 123896−123902.
(26) Chen, H.; Shi, D.; Qi, J.; Wang, B. Structure, Electronic, and Magnetic Properties of Cr-Doped $(ZnS)_{12}$ Clusters: A First-Principles study. *Phys. Lett. A* **2010**, *374*, 4133−4139.
(27) Liu, N.; Zhou, S.; Zhao, J. Solar Driven CO_2 Hydrogenation on Transition Metal Doped $Zn_{12}O_{12}$ Cluster. *J. Chem. Phys.* **2020**, *153*, 164306−164314.
(28) Matxain, J. M.; Formoso, E.; Mercero, J. M.; Piris, M.; Lopez, X.; Ugalde, J. M. Magnetic Endohedral Transition-Metal-Doped Semiconducting-Nanoclusters. *Chem. - Eur. J.* **2008**, *14*, 8547−8554.
(29) Jimenez-Izal, E.; Matxain, J. M.; Piris, M.; Ugalde, J. M. Thermal Stability of Endohedral First-Row Transition-Metal TM@Zn_iS_i Structures, i = 12, 16. *J. Phys. Chem. C* **2011**, *115*, 7829−7835.
(30) Frisch, M. J.; Trucks, G. W.; Schlegel, H. B.; Scuseria, G. E.; Robb, M. A.; Cheeseman, J. R.; Scalmani, G.; Barone, V.; Petersson, G. A.; Nakatsuji, H.; Li, X.; Caricato, M.; Marenich, A.; Bloino, J.; Janesko, B. G.; Gomperts, R.; Mennucci, B.; Hratchian, H. P.; Ortiz, J. V.; Izmaylov, A. F.; Sonnenberg, F. L.; Williams-Young, D.; Ding, F.; Lipparini, F.; Egidi, F.; Goings, J.; Peng, B.; Petrone, A.; Henderson, T.; Ranasinghe, D.; Zakrzewski, V. G.; Gao, J.; Rega, N.; Zheng, G.; Liang, W.; Hada, M.; Ehara, M.; Toyota, K.; Fukuda, R.; Hasegawa, J.; Ishida, M.; Nakajima, T.; Honda, Y.; Kitao, O.; Nakai, H.; Vreven, T.; Throssell, K.; Montgomery, J. A.; Peralta, J. E.; Ogliaro, F.; Bearpark, M.; Heyd, J. J.; Brothers, E.; Kudin, K. N.; Staroverov, V. N.; Keith, T.; Kobayashi, R.; Normand, J.; Raghavachari, K.; Rendell, A.; Burant, J. C.; Iyengar, S. S.; Tomasi, J.; Cossi, M.; Millam, J. M.; Klene, M.; Adamo, C.; Cammi, R.; Ochterski, J. W.; Martin, R. L.; Morokuma, K.; Farkas, O.; Foresman, J. B.; Fox, D. J. *Gaussian 09*, Revision A.02; Gaussian, Inc.: Wallingford, CT, 2016.
(31) Stevens, W. J.; Krauss, M.; Basch, H.; Jasien, P. G. Relativistic Compact Effective Potentials and Efficient, Shared Exponent Basis Sets for the Third, Fourth and Fifth Row Atoms. *Can. J. Chem.* **1992**, *70*, 612−630.
(32) Dolg, M.; Wedig, U.; Stoll, H.; Preuss, H. Energy-Adjusted Ab Initio Pseudopotentials for the First Row Transition Elements. *J. Chem. Phys.* **1987**, *86*, 866−872.
(33) Martin, J. M. L.; Sundermann, A. Correlation Consistent Valence Basis Sets for Use with the Stuttgart-Dresden-Bonn Relativistic Effective Core Potentials: The Atoms Ga-Kr and In-Xe. *J. Chem. Phys.* **2001**, *114*, 3408−3420.
(34) Frisch, M. J.; Head-Gordon, M.; Pople, J. A. Direct MP2 Gradient Method. *Chem. Phys. Lett.* **1990**, *166*, 275−280.
(35) Frisch, M. J.; Head-Gordon, M.; Pople, J. A. Semi-Direct Algorithms for the MP2 Energy and Gradient. *Chem. Phys. Lett.* **1990**, *166*, 281−289.
(36) Head-Gordon, M.; Pople, J. A.; Frisch, M. J. MP2 Energy Evaluation by Direct Methods. *Chem. Phys. Lett.* **1988**, *153*, 503−506.
(37) Saebø, S.; Almlöf, J. Avoiding the Integral Storage Bottleneck in LCAO Calculations of Electron Correlation. *Chem. Phys. Lett.* **1989**, *154*, 83−89.
(38) Head-Gordon, M.; Head-Gordon, T. Analytic MP2 Frequencies Without Fifth Order Storage: Theory and Application to Bifurcated Hydrogen Bonds in the Water Hexamer. *Chem. Phys. Lett.* **1994**, *220*, 122−128.
(39) Becke, A. D. Density-Functional Thermochemistry. III. The Role of Exact Exchange. *J. Chem. Phys.* **1993**, *98*, 5648−52.
(40) Yanai, T.; Tew, D.; Handy, N. A New Hybrid Exchange-Correlation Functional Using the Coulomb-Attenuating Method (CAM-B3LYP). *Chem. Phys. Lett.* **2004**, *393*, 51−57.
(41) Zhao, Y.; Truhlar, D. G. The M06 Suite of Density Functionals for Main Group Thermochemistry, Thermochemical Kinetics, Noncovalent Interactions, Excited States, and Transition Elements: Two New Functionals and Systematic Testing of Four M06-class Functionals and 12 Other Functionals. *Theor. Chem. Acc.* **2008**, *120*, 215−41.
(42) Chai, J.-D.; Head-Gordon, M. Long-Range Corrected Hybrid Density Functionals with Damped Atom-Atom Dispersion Corrections. *Phys. Chem. Chem. Phys.* **2008**, *10*, 6615−20.

https://doi.org/10.1021/acsomega.1c02016
ACS Omega 2021, 6, 16612−16622

(43) Perdew, J. P.; Burke, K.; Ernzerhof, M. Generalized Gradient Approximation Made Simple. *Phys. Rev. Lett.* **1996**, *77*, 3865−68.
(44) Perdew, J. P.; Burke, K.; Ernzerhof, M. Errata: Generalized Gradient Approximation Made Simple. *Phys. Rev. Lett.* **1997**, *78*, 1396.
(45) Grimme, S.; Ehrlich, S.; Goerigk, L. Effect of the Damping Function in Dispersion Corrected Density Functional Theory. *J. Comput. Chem.* **2011**, *32*, 1456−65.
(46) Grimme, S. Semiempirical Hybrid Density Functional with Perturbative Second-Order Correlation. *J. Chem. Phys.* **2006**, *124*, 034108−034123.
(47) Schwabe, T.; Grimme, S. Towards Chemical Accuracy for the Thermodynamics of Large Molecules: New Hybrid Density Functionals Including Non-Local Correlation Effects. *Phys. Chem. Chem. Phys.* **2006**, *8*, 4398−4401.
(48) Schwabe, T.; Grimme, S. Double-Hybrid Density Functionals with Long-Range Dispersion Corrections: Higher Accuracy and Extended Applicability. *Phys. Chem. Chem. Phys.* **2007**, *9*, 3397−3406.
(49) Goerigk, L.; Grimme, S. Efficient and Accurate Double-Hybrid-Meta-GGA Density Functionals—Evaluation with the Extended GMTKN30 Database for General Main Group Thermochemistry, Kinetics, and Noncovalent Interactions. *J. Chem. Theory Comput.* **2011**, *7*, 291−309.
(50) Kozuch, S.; Martin, J. M. L. DSD-PBEP86: In Search of the Best Double-Hybrid DFT with Spin-Component Scaled MP2 and Dispersion Corrections. *Phys. Chem. Chem. Phys.* **2011**, *13*, 20104−20107.
(51) Kozuch, S.; Martin, J. M. L. Spin-Component-Scaled Double Hybrids: An Extensive Search for the Best Fifth-Rung Functionals Blending DFT and Perturbation Theory. *J. Comput. Chem.* **2013**, *34*, 2327−2344.
(52) Brémond, É.; Adamo, C. Seeking for Parameter-Free Double-Hybrid Functionals: The PBE0-DH Model. *J. Chem. Phys.* **2011**, *135*, 024106−024111.
(53) Brémond, É.; Sancho-García, J. C.; Pérez-Jiménez, Á. J.; Adamo, C. Communication: Double-Hybrid Functionals From Adiabatic-Connection: The QIDH Model. *J. Chem. Phys.* **2014**, *141*, 031101.
(54) Boto, R. A.; Peccati, F.; Laplaza, R.; Quan, C.; Carbone, A.; Piquemal, J.-P.; Maday, Y.; Contreras-Garcia, J. NCIPLOT4: Fast, Robust, and Quantitative Analysis of Noncovalent Interactions. *J. Chem. Theory Comput.* **2020**, *16* (7), 4150−4158.
(55) Johnson, E. R.; Keinan, S.; Mori-Sanchez, P.; Contreras-Garcia, J.; Cohen, A. J.; Yang, W. Revealing Non-Covalent Interactions in Solids: NCI Plots Revisited. *J. Am. Chem. Soc.* **2010**, *132*, 6498−6506.
(56) Contreras-Garcia, J.; Johnson, E. R.; Keinan, S.; Chaudret, R.; Piquemal, J.-P.; Beratan, D. N.; Yang, W. NCIPLOT: A Program For Plotting Noncovalent Interaction Regions. *J. Chem. Theory Comput.* **2011**, *7*, 625−632.
(57) Deglmann, P.; May, K.; Furche, F.; Ahlrichs, R. Nuclear Second Analytical Derivative Calculations Using Auxiliary Basis Set Expansions. *Chem. Phys. Lett.* **2004**, *384*, 103−107.
(58) Eichkorn, K.; Treutler, O.; Öhm, H.; Häser, M.; Ahlrichs, M. Auxiliary Basis Sets to Approximate Coulomb Potentials. *Chem. Phys. Lett.* **1995**, *240*, 283−290.
(59) Sierka, M.; Hogekamp, A.; Ahlrichs, R. Fast Evaluation of the Coulomb Potential for Electron Densities Using Multipole Accelerated Resolution of Identity Approximation. *J. Chem. Phys.* **2003**, *118*, 9136−9148.
(60) *TURBOMOLE*, Version 6.6 a; Development of University of Karlsruhe and Forschungszentrum Karlsruhe GmbH, 1989−2007, TURBOMOLE GmbH, 2007, available from http://www.turbomole.com.

https://doi.org/10.1021/acsomega.1c02016
ACS Omega 2021, 6, 16612−16622